

Ionic mechanisms of membrane excitability and electrical signal transduction between cells

J. W. MOZRZYMAS

*Department of Biophysics
Wrocław Medical University
ul. Chatubińskiego 10, 50-368 Wrocław
mozrzy@biofiz.am.wroc.pl*

1. Introduction and aims of this work

Fast signaling within a single neuron is based predominantly on transmission of electrical signals [1]. Quick communication between neurons involves additionally a chemical compound called neurotransmitter. The general rule is that the electrical signal travels a long distance on an axon or dendrite (Fig. 1), while neurotransmitter act only at a very short range within the synapse. The transduction of electrical signals in chemical synapses is the most fundamental mechanism of fast signaling in the adult central nervous system. Motor activity is also “commanded” by chemical synapses at the neuromuscular junctions.

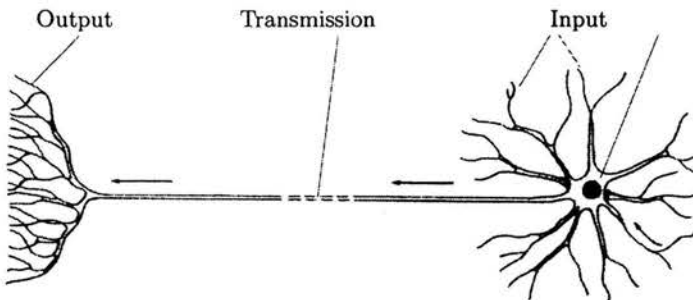


FIGURE 1. Schematic view of a neuron.

Understanding of the mechanisms underlying the synaptic transmission is therefore of primary interest. It is known that electrical signaling is based on the ion transport through the cell membrane. The ability of the cell membrane to conduct selectively different ions and to effectively regulate its permeability to ions within very short times underlies a large variety of signaling patterns in the living cells. The development of electrophysiological techniques provided a powerful tool that allowed a considerable insight into the mechanisms underlying the electrical activity of living cells [2]. However, these phenomena are so complex that measurement of, e.g. electrical potentials, was insufficient to fully describe these processes. In the attempts to explore the nature of electrical signals in cell membranes, mathematical and physical modeling gave a substantial contribution [3]. This concerned both the macroscopic phenomena (as e.g. action potentials) as well as microscopic ones occurring at the single channel level. The aim of this review is to highlight some aspects of modeling in the field of electrical signal transduction in neurons. This will consist of a presentation of a background theory on electrodiffusion of ions through the biological membranes and on the analysis of the mechanisms underlying the action potentials and synaptic currents. A particular attention will be paid to the processes accompanying the synaptic transmission. Such model and quantitative investigations will be presented in strict relation to the experimental evidence and experimental techniques. Investigations based on model simulations performed in parallel with experiment is a common approach enabling to verify previous hypotheses and propose new ones. Especially in the case of analysis of electrical signaling such approach proved extremely useful. Often the first approach to test the proposed hypothesis was an attempt to make an extrapolation of the present knowledge using the model simulations. The major challenge in electrophysiology was insufficient resolution of recordings that made it difficult to interpret the data in terms of molecular mechanisms. Electrophysiological approaches were used for over 30 years before recordings at the single channel level became available. However, we observe that most of information that emerged after introduction of the patch-clamp technique, were quite well understood before. This was due to advanced analytical methods often based on model considerations.

2. Membrane voltage is the main carrier of quickly transferred information

Membrane voltage is defined as potential difference between the interior and exterior of the cell:

$$V_m = V_{in} - V_{out}, \quad (2.1)$$

where V_m is the membrane voltage (called also membrane potential), V_{in} is the potential of the cell interior and V_{out} is the potential outside the cell.

The membrane potential can be measured using a thin (so-called also “sharp”) electrode method that was introduced by Fatt and Katz in late thirties [4]. The principle of this technique is shown schematically in Fig. 2. The concept of this method is very simple: we have to “connect” one electrodes

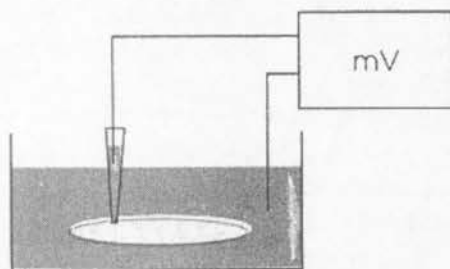


FIGURE 2. Recordings of the membrane voltage; adapted from [5].

to the cell interior and the second one immerse in the washing external solution. The major problem was to make a sufficiently good electrical contact with the cytoplasm without excessive damaging the cell membrane. This task has been achieved by using very thin glass electrodes (tip diameter less than $1\ \mu\text{m}$). Initially the problems with a large tip resistance (and related potential drop) was encountered but this difficulty was eliminated by using highly conducting electrode filling electrolyte (3 M KCl).

The resting membrane potential, measured using this technique (on e.g. squid giant axon) were approximately $-65\ \text{mV}$. The value of the resting membrane voltage for different cell types may show considerable differences (e.g. for muscle fibers it is approximately $-90\ \text{mV}$) but it is a general rule that it is negative and accounts for several tens of millivolts. The value of membrane potential might look not very large as we are used to deal with voltages measured at least in volts. However, it needs to be taken into account that this potential difference occurs at the distance equal to the width of the cell membrane (approx. $10\ \text{nm}$). Simple application of the relationship between the intensity of the electrical field and potential gradient ($E = -\Delta V/\Delta x$) indicates that the field intensity in the biological membranes is really enormous: $10^7\ \text{V/m}$. Such strong electrical fields are necessary to effectively command processes underlying membrane excitability.

The main question after the discovery of the resting membrane voltage concerned the mechanism underlying the maintenance of the constant value of the membrane potential. This problem is addressed in the next chapter in

which the physical model of membrane is proposed and the electrodiffusion theory is discussed.

2.1. Membrane voltage and ionic transport through the biological membranes in the resting state

The mechanism of ion transport through biological membranes is based on two basic processes: diffusion and migration in the electrical field. Thus these processes are superimposed on each other and the resulting phenomenon is defined as electrodiffusion.

Diffusion process is described by the Fick law:

$$J = -D \frac{dc}{dx}, \quad (2.2)$$

where J is the flux density, D – diffusion coefficient, c – local concentration, x – position. For the considerations restricted to the membrane transport this equation can be rewritten as follows:

$$J = -\frac{\beta D}{l} \Delta c, \quad (2.3)$$

where β is the partition coefficient, l is the membrane thickness and Δc is the concentration difference between the inner and outer side of the membrane.

The constants on the right hand side of the (Eq. 2.3), can be defined as follows:

$$P = \frac{\beta D}{l}, \quad (2.4)$$

where P is the permeability coefficient.

The migration of ions in the electrical field is described by so-called Ohm's law in the differential form:

$$J = -\sigma \frac{dV}{dx} = -nzu \frac{dV}{dx}, \quad (2.5)$$

where J is the flux density, σ – conductivity, u – mobility, n – concentration of ions (number/volume), z – valency, V – local electrical potential, x – position.

In electrophysiological experiments it is easier to measure the current density j ($j = zeJ$) and using molar concentration ($n = N_a \cdot c$) are more commonly used. Then Eq. (2.5), may be rewritten in the following form:

$$j = -z^2 c F u \frac{dV}{dx} = -\sigma \frac{dV}{dx}, \quad (2.6)$$

where F is the Faraday constant ($F = N_a \cdot e$, e - elementary charge).

The Fick law (see (Eq. 2.2) can be rewritten for the current density:

$$j_{\text{dif}} = -zFD \frac{dc}{dx}. \quad (2.7)$$

The formulas (2.4) and (2.6) represent the contributions from the process of migration in the electrical field and therefore diffusion to the overall flux of ions in the electrolyte that is given by the following relationship:

$$j = j_{\text{dif}} + j_{\text{el}} = -zFD \frac{dc}{dx} - z^2cFu \frac{dV}{dx}, \quad (2.8)$$

where j_{dif} and j_{el} are the flux components due to the diffusion and migration in electric field, respectively. Taking into account the relationship between the diffusion and mobility coefficients:

$$u = \frac{F}{RT}D. \quad (2.9)$$

The equation for the current density takes form:

$$j = -zFD \left(\frac{dc}{dx} + \frac{zFc}{RT} \frac{dV}{dx} \right). \quad (2.10)$$

The Equation (2.9) represents the Nernst–Planck equation for electrodiffusion.

The simplest case – equilibrium

In the case in which the diffusional flux of a considered ion has the same absolute value as the one resulting from the migration in the electrical field but the opposite direction, the net flux of electrical charge is zero. Such situation correspond to the so-called Nernst equilibrium. In this case Eq. (2.9) takes form:

$$\frac{RT}{zF} \frac{1}{c} \frac{dc}{dx} = \frac{dV}{dx}, \quad (2.11)$$

that, after integration with respect to the position variable x within the limits describing the membrane thickness yields (T is the absolute temperature):

$$V_{\text{eq}} = \frac{RT}{zF} \ln \frac{c_{\text{out}}}{c_{\text{in}}}. \quad (2.12)$$

The equilibrium potentials for different ions may vary from cell to cell but typical values are the following: -95 mV for potassium ions, 45 mV for sodium ions, -70 mV for chloride ions. Thus, for a given type of ion, the flux intensity depends on the distance of the membrane voltage from the equilibrium

potential ($V - V_{eq}$). This parameter is named the electrical driving force for an ion. The situation corresponding to ion flux that becomes zero at the equilibrium Nernst potential and its intensity is proportional to the electrical driving force can be modeled using the electrical equivalent circuit in the form:



FIGURE 3. Equivalent electrical circuit reproducing the situation in which the ion flux is proportional to the electrical driving force and becomes zero at the Nernst potential.

The resistor R represents the resistance of the membrane permeant for a given ion. More commonly the conductance $G = 1/R$ is used. Membrane conductance is proportional to the permeability of the membrane.

Resting membrane potential does not represent the equilibrium

The investigations presented above indicate that when the membrane is permeable to only one ion, the membrane voltage will equilibrate reaching the value described by the Nernst Eq. (2.12). However, biological membranes show non-zero permeability to different ions (e.g. sodium, potassium, chloride, etc.) and as mentioned above all these ions are characterized by different Nernst potential. In this situation there is no possibility for the system to reach the Nernst equilibrium. For instance, when the membrane potential reaches the Nernst potential for the potassium ions ($V_K = -95$ mV), then the sodium ions are very distant from the equilibrium. In this situation, the only possibility to maintain the constant value of the membrane potential is that the net current is equal zero while the respective ionic fluxes are non-zero but compensate each other:

$$j = j_K + j_{Na} + j_{Cl} + \dots = 0. \quad (2.13)$$

The calculation of each of the components of the ionic flux requires integration of the Nernst–Planck Eq. (2.10). Below, I present a derivation of the Nernst–Planck equation for the conditions believed to reasonably mimic the situation in the biological membrane.

Let us multiply both sides of Eq. (2.10): by $\exp(zFV/RT)/D$. And after some simple algebra we get:

$$j(\exp(zFV/RT)/D) = -zF \frac{d}{dx} (c \cdot \exp(zFV/RT)/D). \quad (2.14)$$

We may now perform integration within the range of the variable x corresponding to the width of the membrane. To include in these investigations that the considered ion may have different solubility in the bulk solution and in the membrane we have assumed that the concentration of ion within the membrane is given by $\beta \cdot c$, where β is the partition coefficient. Thus, taking this into account, the Eq. (2.14) can be rearranged as follows:

$$j \int_0^d (\exp(zFV/RT)/D) dx = -zF\beta (c_{in} \exp(zFV/RT)/D - c_{out}). \quad (2.15)$$

Hence we get:

$$j = -zF\beta \frac{c_{in} \exp(zFV_m/RT)/D - c_{out}}{\int_0^d (\exp(zFV/RT)/D) dx}, \quad (2.16)$$

where V_m is the membrane potential.

Integration of Eq. (2.16) requires knowledge of the potential profile $V(x)$ across the membrane. Assuming that the intensity of the electrical field within the membrane is constant (that is equivalent to the linear dependence of potential on position) the integration in the denominator of the Eq. (2.16) can be easily performed and the formula for the flux takes form:

$$j = -zF\beta \frac{c_{in} \exp(zFV_m/RT)/D - c_{out}}{\frac{RTd}{zDFV_m} (1 - \exp(-zFV_m/RT))}. \quad (2.17)$$

Equation (2.17) represents the so-called constant field equation of ion flux.

In an analogous way we may determine the fluxes for all the considered ions and calculate the value of the membrane potential V_m that would satisfy the conditions describing the resting membrane potential (Eq. (2.13). Taking into consideration the definition of the permeability coefficient P (see Eq. (2.4) and after some algebra we obtain:

$$j = 0 = \frac{V_m F^2}{RT(1 - \exp(-zFV_m/RT))} (P_{Na} c_{Na}^{in} + P_K c_K^{in} + P_{Cl} c_{Cl}^{out} - (P_{Na} c_{Na}^{out} + P_K c_K^{out} + P_{Cl} c_{Cl}^{in}) \exp(-V_m F/RT)). \quad (2.18)$$

The membrane potential V_m can be easily obtained by solving this equation:

$$V_m = \frac{RT}{F} \ln \frac{P_{\text{Na}}c_{\text{Na}}^{\text{out}} + P_{\text{K}}c_{\text{K}}^{\text{out}} + P_{\text{Cl}}c_{\text{Cl}}^{\text{in}}}{P_{\text{Na}}c_{\text{Na}}^{\text{in}} + P_{\text{K}}c_{\text{K}}^{\text{in}} + P_{\text{Cl}}c_{\text{Cl}}^{\text{out}}}. \quad (2.19)$$

Equation (2.19) describes the resting potential in conditions in which the membrane is permeable for three considered ions (K, Na, Cl) and the permeability for each ion is measured by the respective permeability coefficient P , and the concentrations of ions in both intra- and extracellular side are known. This equation is commonly named in the relevant literature as Goldman-Hodgkin-Katz equation.

Potassium electrode theory

It is known that at rest, the membrane show largest permeability for potassium ions. When assuming that $P_{\text{K}} \gg P_{\text{Na}}$ and $P_{\text{K}} \gg P_{\text{Cl}}$ (i.e. the permeabilities for sodium and chloride ions are negligible with respect to the one for potassium), then Eq. (2.19) simplifies to the form of the Nernst potential for potassium ions:

$$V_m = \frac{RT}{F} \ln \frac{c_{\text{K}}^{\text{out}}}{c_{\text{K}}^{\text{in}}}. \quad (2.20)$$

This illustrates the correspondence between the situation in which the permeability for one ion becomes predominant and assumptions underlying the equilibrium Nernst potential are satisfied.

It is known that biological membranes in the resting conditions exhibit the largest permeability for potassium ions. Using this property of the membranes, early theories proposed that the resting membrane potential represent the equilibrium potential for potassium ions (so-called potassium electrode theory). However, more precise measurements of membrane voltage demonstrated that in physiological conditions it was not correct. The experimental test for the potassium electrode theory relied on measurement of the membrane voltage using sharp electrodes at various concentrations of extracellular concentrations of potassium ions. The measured potentials were confronted with predictions of the Nernst potentials (Eq. (2.20)). For a wide range of concentrations ($c_{\text{K}} > 10 \text{ mM}$) the dependence of measured potentials on c_{K} was in agreement with prediction of the Nernst theory. However, at lower values of c_{K} , there was a significant discrepancy between the measured membrane voltage and the calculated Nernst equation. This discrepancy has been demonstrated to result from contributions of fluxes of other ions (e.g. sodium and chloride). Since the physiological concentration of extracellular potassium ions is much lower than 10 mM (approximately 2 mM), it is now

generally accepted that the Goldman–Hodgkin–Katz (GHK) formula is much more useful for the description of the membrane resting potential than the Nernst equation.

2.2. Hodgkin and Huxley’s description of the action potential

Excitable cells (muscle fibers and neurons) show a capacity to produce impulse-like signals called action potentials. This phenomenon has been first observed in the forties of the last century by Cole and Curtis [4] and later has been systematically described by Hodgkin and Huxley [6-10]. The action potentials have been measured with the same technique that has been used for recordings of the resting membrane potentials (Fig. 2). The time course of the action potential is extremely fast: the value of the membrane potential changes by nearly 100 mV within approximately 1 ms. The return to the resting state is also very fast although slower than the onset (Fig. 4).

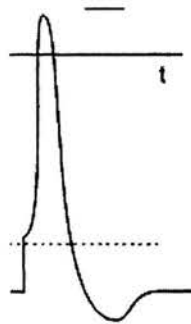


FIGURE 4. The time course of the action potential. Scale bar represents 1 ms period.

Later studies have demonstrated that this phenomenon is of fundamental importance. Action potentials are universal carriers of the fast signals at long distances (e.g. in axons of motoneurons action potentials often “travel” for more than 1 m). It is interesting that the waveform of action potentials is greatly preserved among different types of neurons and even different species. This implies that, from the point of view of information transfer in neurons, its kinetics is not of primary importance and several studies indicate that the information is encoded rather in the frequency of action potentials. Action potential can be regarded thus as a basic unit of information transferred within a neuron.

It is not therefore surprising that this phenomenon attracted much attention of investigators not only in the field of biology and physiology but also in physics and mathematics.

The approach employed by Hodgkin and Huxley in the fifties to explore the mechanisms of action potential remains one of the most superb examples of ingenious investigations in this field of science. In particular, the strength of their work consisted of the use of very elegant experimental approach (voltage-clamp and intracellular recordings) and very insightful application of quantitative data elaboration using model simulations. The method used by them in the fifties is one of very few that remains in use with little modifications. The so-called Hodgkin and Huxley's equations remain the basic tool in quantitative description of action potential and underlying currents. From the mathematical point of view the Hodgkin and Huxley's equations describing the non space clamp conditions (see below) are so complex (system of partial differential equations) that generations of mathematicians were involved in investigations of various boundary problems described by this formalism.

Action potential is a threshold phenomenon

In the excitable cells (neurons, muscle fibres) the membrane potentials continuously fluctuates around the resting state. Such temporal variation of the membrane voltage is most clearly manifested in neurons in which the dendrites and soma may receive thousands of synaptic signals within one second. These signals are integrated in space and time giving rise to different patterns of neuronal activity. The basic question regarding the action potential was to understand the criterion when it may be evoked. As found by pioneers of electrophysiology in the late forties, a sufficient stimulus to evoke the action potential is to cross the so-called threshold value of the membrane voltage

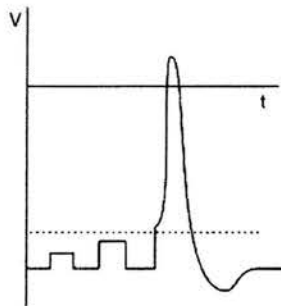


FIGURE 5. When changes of membrane potential occur below the threshold value (dashed line) action potential cannot be evoked. When the membrane voltage exceeds the threshold the action potential appears in the "all or nothing" fashion.

that typically is around -50 mV. This means that when the membrane voltage fluctuates below the threshold, no action potential occurs but as soon as the threshold is crossed, this phenomenon is initiated (Fig. 5). After crossing the threshold values, the time course of the action potential is very similar independently of how strong was the suprathreshold stimulus. This implies that the action potential appears either in its "standard" form or is absent. This led to a definition that appearance of action potential is ruled by an "all or nothing" principle.

Mechanisms underlying the action potential

Figure 6 shows a typical experiment in which the action potential is evoked in an excitable cell (squid giant axon).

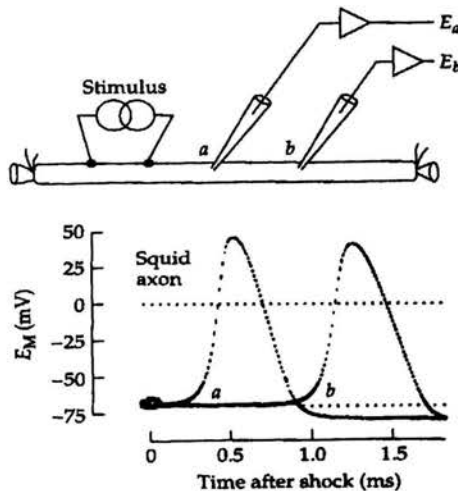


FIGURE 6. Recordings of action potential. "Stimulus" represent an electrode able to evoke the action potential that is measured by two electrodes impaled along the axon. Traces below show the time course of the action potential measured by the electrodes "a" and "b"; adapted from [2].

Thus, using the standard intracellular recording technique we may measure the time course of the action potential with a good time resolution. Note that when placing the electrodes at various known distances one from another it is possible to additionally assess the velocity of action potential propagation that for the squid giant axon is approximately 20 m/s. From the electrodiffusion background it is clear that the variation of the membrane

voltage during the action potential must result from the flow of ions through the axonal membrane. From early experiments in which the concentrations of various ions (mainly sodium and potassium) was varied, it became clear that the rising phase of the action potential is related to the flux of sodium, while the decay depends on the potassium ions. It was thus deduced that such rapid onset of the action potential resulted from a sudden influx of sodium ions. Since it is known that there is a large electrochemical gradient for sodium ions (much larger $[Na]_{out}$ than $[Na]_{in}$) such mechanism strongly suggested a rapid increase in the sodium conductance of the axonal membrane after crossing the threshold value. Thus, the increase in the membrane conductance would be caused by a rise in the membrane potentials indicating a voltage-sensitive processes. Although the experiments presented above provided good qualitative indications, these recordings (such as in Fig. 6 in the presence of extracellular salines with different ion compositions) bring insufficient information to provide a full quantitative description of the currents underlying the action potential. Let us note that the description of the action potential would require a contemporary measurement voltage as well as of sodium and potassium currents while by using the intracellular recording technique we are able to measure only one of them: time course of the membrane voltage (Fig. 6). Hodgkin and Huxley have designed an ingenious solution to obtain the lacking information: membrane currents. They have applied the so-called voltage-clamp technique that allows to measure the ionic currents flowing through the entire cell membrane while the membrane voltage is controlled by the experimenter. Typical results of experiment carried out using this technique is shown in Fig. 7. The membrane voltage (V_m) is kept at a negative value corresponding to the resting membrane potential (-60 mV) and then a sudden, square-like voltage depolarization is applied. As shown in the bottom trace of Fig. 7 ($I_K + I_{Na}$) such depolarizing pulse elicits a biphasic (first negative – inward and then positive – outward) currents. Such components of currents have been ascribed to the sodium (inward) and potassium (outward) currents. These components can hardly be separated basing only on these electrophysiological recordings (the device measures the flow of electrical charges without any possibility to distinguish the sodium ion from the potassium one). The separation between these current components became possible due to application of toxins that selectively block sodium and potassium membrane conductances. Thus, when applying the blocker of sodium conductance (tetrodotoxin, TTX), only the potassium current component remained (I_K). Similarly, when applying tetraethylamine (TEA), the potassium component is blocked and the sodium current (I_{Na}) can be measured.

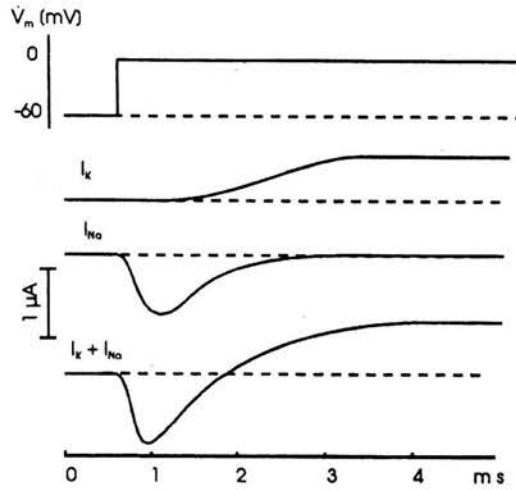


FIGURE 7. Examples of voltage-clamp recordings. Membrane voltage is clamped at -60 mV and the depolarizing square-like pulse is applied. Total biphasic current is recorded (bottom trace $I_K + I_{Na}$ is recorded). To separate the underlying sodium and potassium components (I_K and I_{Na} , respectively) the respective toxins are applied (TTX blocks sodium and TEA) potassium currents; adapted from [5].

Let us note that assuming that the values of the equilibrium potential for sodium and potassium ions (E_{Na} , E_K) are known, using the voltage clamp technique, we are able to measure the currents at known values of the electrical driving forces for these ions ($V - V_{Na}$ and $V - V_K$). This implies that the measured currents provide direct information on respective chord conductances (see Eqs. (2.21 and 2.22)):

$$g_{Na}(t, V) = \frac{j_{Na}(t, V)}{V - V_{Na}}, \quad (2.21)$$

$$g_K(t, V) = \frac{j_K(t, V)}{V - V_K}. \quad (2.22)$$

Thus, the application of the voltage - clamp technique allowed to determine the kinetics and voltage-dependencies of the sodium and potassium conductances in the excitable cells (Fig. 8). As it will be described in details below, the results presented in Fig. 8 contain crucial information to provide a quantitative description of the action potential phenomenon.

Let us note that the sodium conductance shows a faster onset in response to the voltage step than the potassium one (compare panels A and B in Fig. 8). However, after a few milliseconds the sodium conductance declines

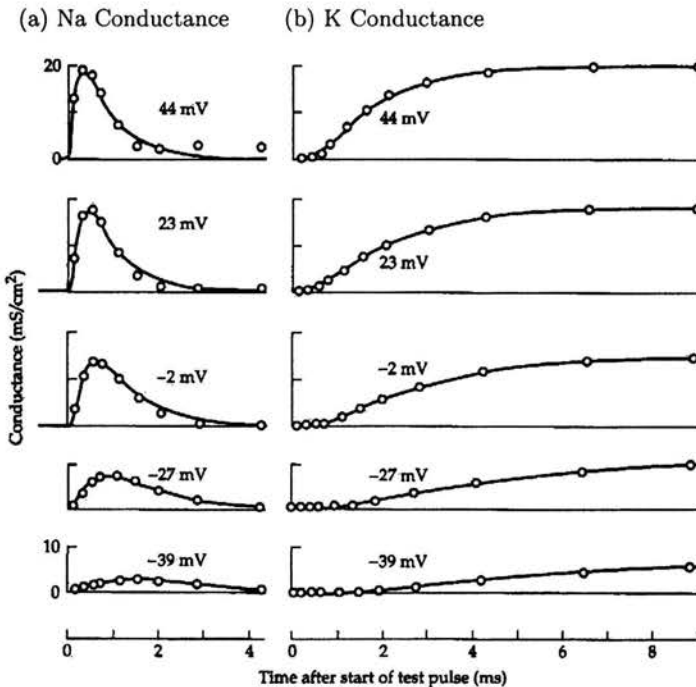


FIGURE 8. Time course of the voltage-dependencies of the sodium (a) and potassium (b) conductancies evoked by step-like voltage pulses (duration of the depolarizing square pulse cover entire time scale presented in the figure); adapted from [2].

in spite of the presence of the depolarizing stimulus. This phenomenon of progressive loss of activity during a prolonged exposure to the depolarization is defined as inactivation.

Hodgkin and Huxley equations provide the analytical frame to describe the action potential

The experimental evidence based on the intracellular recordings of the membrane potential (Figs. 4 and 6) and on current measurement using the voltage-clamp technique (Figs. 7 and 8) provided empirical background to study the mechanisms underlying the phenomenon of the action potential. To fully explore this phenomenon in physical terms, Hodgkin and Huxley proposed the model that enabled them to provide one of the most successful and most frequently used quantitative description of electrical signals in biological systems. The Hodgkin and Huxley's investigations were based on a relatively simple considerations of the electrodiffusion theory. It is assumed

that in the simplest case the membrane consists of a resistor and capacitor and therefore the total current is a sum of a “ohmic” and capacitive (displacement) currents (Figs. 9 and 6):

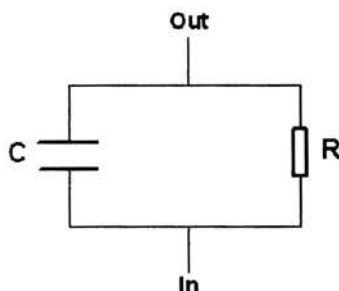


FIGURE 9. Simple equivalent electrical circuit assuming parallel connection of a capacitor and resistor.

$$j = C \frac{dV}{dt} + gV, \quad (2.23)$$

where $g = 1/R$ (conductance) and V – membrane potential.

In a more realistic case we have to consider that the membrane is selectively permeable to different ions. This fact requires inclusion in the model in Fig. 9 at least 3 conductances (sodium g_{Na} , potassium g_K and aspecific leakage g_L) and the equilibrium potentials for these conductances are modeled by respective electromotive forces (Fig. 10).

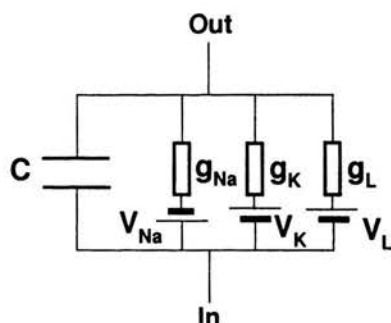


FIGURE 10. Equivalent electrical circuit for a membrane in which selective pathways for sodium and potassium ions are assumed. g_L and V_L represent the conductance and reversal potential for the leakage component of ionic currents.

For the circuit presented in Fig. 10, Eq. (2.23) needs to be rewritten in the form:

$$j = C \frac{dV}{dt} + g_{Na}(V - V_{Na}) + g_K(V - V_K) + g_L(V - V_L). \quad (2.24)$$

Assuming that there are no external sources of current (e.g. external electrodes) the total current j is zero that is equivalent to the statement that the ionic currents flowing through the membrane charge the membrane capacitor C :

$$C \frac{dV}{dt} = -g_{Na}(V - V_{Na}) - g_K(V - V_K) - g_L(V - V_L). \quad (2.25)$$

As indicated by the voltage-clamp experiments (Eqs. (2.24) and (2.25)), the sodium and potassium conductances $g_{Na}(V, t)$ and $g_K(V, t)$ need to be regarded as functions of the membrane voltage V and time.

The Equations (2.24) and (2.25) represent a simple charge balance for the membrane. However, the most difficult step was to find optimally fitting functions for strongly voltage-dependent sodium and potassium conductances $g_{Na}(V, t)$ and $g_K(V, t)$. Below I report the strategy employed by Hodgkin and Huxley to solve this problem. The functions describing sodium and potassium conductances were defined as follows:

$$\begin{aligned} g_{Na}(V, t) &= g_{Na}^o m^3(V, t) h(V, t), \\ g_K(V, t) &= g_K^o n^4(V, t), \end{aligned} \quad (2.26)$$

where g^o represent the maximum sodium and potassium conductances, $m(V, t)$ and $h(V, t)$ represent the functions describing activation and inactivation process of the sodium conductance, $n(V, t)$ is the function describing the activation of the potassium conductance (in the classical experiments on squid giant axon, the potassium conductance did not show any considerable inactivation in the time scale of the action potential).

Each of the m , h and n functions are assumed to be described by the first order reaction equation:

$$\begin{aligned} \frac{dm}{dt} &= \alpha_m(1 - m) - \beta_m m, \\ \frac{dh}{dt} &= \alpha_h(1 - h) - \beta_h h, \\ \frac{dn}{dt} &= \alpha_n(1 - n) - \beta_n n. \end{aligned} \quad (2.27)$$

Each of the α and β coefficients depends on membrane voltage. Thus from the methodological point of view, the Hodgkin and Huxley's equations postulate

the form of the functions describing sodium and potassium conductances by Eqs. (2.26) and (2.27) and the fit to the experiment is obtained by optimal choice of the α and β coefficients for each considered voltage at which the conductances were measured. As a result of this procedure, Hodgkin and Huxley proposed α and β coefficients as strongly non-linear functions of membrane voltage:

$$\begin{aligned} \alpha_m &= \frac{-0.1(V+35)}{e^{-0.1(V+35)} - 1}; & \beta_m &= 4e^{-(V+60)/18}, \\ \alpha_h &= 0.07e^{-0.05(V+60)}; & \beta_h &= \frac{1}{1 + e^{-0.1(V-30)}}, \\ \alpha_n &= \frac{-0.01(V+50)}{e^{-0.1(V+50)} - 1}; & \beta_n &= 0.125e^{-0.0125(V+60)}. \end{aligned} \quad (2.28)$$

Equations (2.25) and (2.28) express complete Hodgkin and Huxley equations that enabled a very good quantitative description of the action potential in the space-clamp conditions (space-clamp means that the membrane potential is assumed to be spatially homogeneous). Although electrophysiologists are now aware about some imperfections in describing the experimental data, the approach based on the Hodgkin and Huxley's equations remains the most basic tool in these investigations. The application of the above mathematical formalism allowed to calculate the time course of the sodium and potassium conductances during the generation of the action potential (Fig. 11).

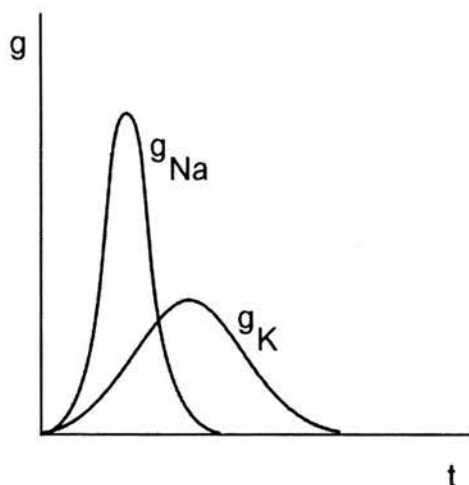


FIGURE 11. Time course of the sodium and potassium conductances during the generation of the action potential.

Hodgkin and Huxley's equation for a propagating wave

Hodgkin and Huxley's equations presented above (Eqs. (2.25) and (2.28)) represent a situation in which the membrane potential is spatially homogeneous. Such situation is typical in the voltage-clamp experiments and is very useful when studying the phenomena underlying the generation of the action potential. However, as discussed above in a real system, the action potentials travel along axons for long distances. Such "travelling" obviously breaks the spatial homogeneity and requires approaching a much more complex problem – solution of the boundary value problem given by the following partial differential equation:

$$C_m \frac{dV}{dt} = \frac{a}{2\rho_i} \frac{\partial^2 V}{\partial x^2} - g_{Na}(V - V_{Na}) - g_K(V - V_K) - g_L(V - V_L), \quad (2.29)$$

where a – the axon radius, ρ_i – the axoplasm resistivity (the remaining parameters are as specified previously).

In the general case the solution of the boundary value problem for the Eq. (2.29) and Eqs. (2.26) and (2.28) is extremely complex and obviously depends on the boundary and initial conditions. However, the observation that the action potential may travel along the axon without changing its kinetic shape led Hodgkin and Huxley to look for a specific 'travelling wave' solutions of these equations. If the 'wave' of action potential is moving rightward with a constant velocity u , then for any time t the solution $V(t_0, x)$ must be equal to $(t_0 + t, x + ut)$.

If we put

$$z = x - ut, \quad (2.30)$$

then

$$\frac{\partial V}{\partial x} = \frac{\partial V}{\partial z} \frac{\partial z}{\partial x} = \frac{\partial V}{\partial z} \quad (2.31)$$

and

$$\frac{\partial V}{\partial t} = \frac{\partial V}{\partial z} \frac{\partial z}{\partial t} = -u \frac{\partial V}{\partial z} \quad (2.32)$$

and the boundary value problem (Eq. (2.29)) reduces to the ordinary differential equation:

$$\frac{d^2 V}{dz^2} + \frac{2Cu\rho_i}{a} \frac{\partial V}{\partial z} = \frac{2\rho_i}{a} [g_{Na}(V - V_{Na}) - g_K(V - V_K) - g_L(V - V_L)]. \quad (2.33)$$

Hodgkin and Huxley have found numerical solutions for Eq. (2.33) for the velocities u comparable to those observed in the experiment.

Stochastic interpretation of Hodgkin and Huxley's equations

We observe that in the Hodgkin and Huxley's formalism the sodium and potassium conductances are proportional to the factors n^3h and n^4 , respectively. The m , h and n functions are normalized to unity (i.e. $0 \leq n \leq 1$) and therefore these parameters can be interpreted in terms of probability. Let us start with the function n^3h describing the sodium conductance and imagine that channel opening relies on the state of 3 locks n and one lock h . Thus a channel opens if all 3 "n" locks are in open position and when "h" lock (describing inactivation) is not in an inactive mode. If the probability of an activation gate type "n" to be in an active position is n , then the probability that three of them will find themselves in an active mode will be n^3 (assuming that they act independently). Consequently, the probability that all three activation gates will be in active mode and additionally the inactivation gate will be in a non-inactivated mode will be n^3h . Similarly, assuming that for potassium channel the activation gate consists of four identical particles n , the probability that all of them will be on the active mode will be n^4 . The above interpretation is referred to the state of a single channel while the Hodgkin and Huxley's equation were used to describe the macroscopic currents. For macroscopic currents (such as measured by Hodgkin and Huxley), n^3h and n^4 represent the fractions of open sodium and potassium channels, respectively. Although in the fifties, when the Hodgkin and Huxley's equations were introduced, the experimental methods did not allow to verify the above interpretation at the single channel level. The introduction of the patch-clamp technique (see below) allowed in mid seventies to record the single channel currents and revealed that single channel activity shows a stochastic nature. More recent studies, using molecular biology and structural tools confirmed the presence of charged structures within channel macromolecules responsible for activation and inactivation processes.

3. Patch-clamp technique reveals the single channel functioning

As described above, the voltage-clamp technique allowed to measure the current flowing through the entire cell membrane but proved insufficient to describe the properties of single channels. It needs to be emphasized that in the fifties, when Hodgkin and Huxley were working on the action potential theory, the ionic channels could be at best a matter of intuition – at that time there were no direct approaches to demonstrate their presence and to describe their properties. Some progress has been achieved in the sixties and early seventies when the so-called noise analysis was introduced [11-13].

This approach has been applied to analyze the current noise induced by low agonist concentration. The key observation coming from these experiments was that increase in conductance induced by low agonist concentrations was associated with a large noise suggesting that the agonist activated discrete currents due to activity of stochastically opening ionic channels. This method provided first insight into the properties of single channels. However, a direct evidence demonstrating the functioning of single channels was lacking. In mid seventies Erwin Neher and Bert Sakmann [14] made one of the most significant breakthrough in the history of physiology – they have introduced a method that allowed to routinely record the activity of single channels. The method was named patch-clamp technique. The concept of this method is similar to that of the voltage-clamp: it allows to measure the current while controlling the membrane potential. Below, I describe the main ideas and concepts related to this technique. The main difference between the classical voltage-clamp and patch-clamp techniques is that in the case of the latter, recordings are restricted to a very small piece of membrane (patch) in which a small number of channels is present. As shown in Fig. 12, the tip of pipette forms a tight contact with the cell membrane. The resistance of this seal reaches hundreds gigaohms (thus so-called gigaseal). The contact is also characterized by high mechanical stability. The pipette is filled with a saline that may contain a desired agonist concentration (in the case of studies of ligand gated channels). The electrode inserted into the pipette is connected to an operational amplifier (triangle in Fig. 12) with a high resistance feedback loop. This system allows to set the pipette potential at the external side of the membrane and to record the current flowing through the patch enclosed by the tip of the electrode. In this way, the area of the cell membrane is limited to the patch underlying the pipette (diameter of approximately 1 – 2 microns).

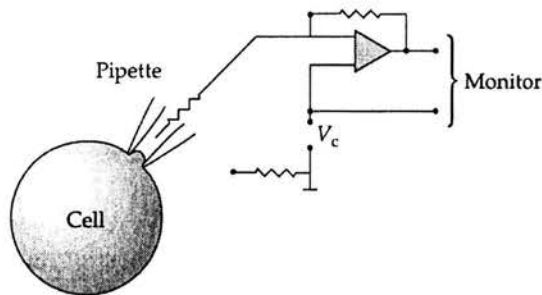


FIGURE 12. Schematic view of the patch-clamp technique in the cell-attached configuration; adapted from [15].

In the situation presented in Fig. 12, the electrical circuit is closed by the rest of the cell membrane and therefore, the resting membrane potential adds to the pipette potential fixed (clamped) at the extracellular side of the membrane:

$$V_m = V_r - V_{\text{pip}}, \quad (3.1)$$

where V_m - membrane potential of the membrane patch, V_r - resting membrane potential V_{pip} - potential of the pipette.

Thus, when lowering the pipette potential, the membrane patch is depolarized and the opposite effect on the membrane voltage is obtained when increasing the pipette potential.

In the cell-attached configuration it is possible to record the single channel activity, as shown in side of the membrane (Fig. 13).

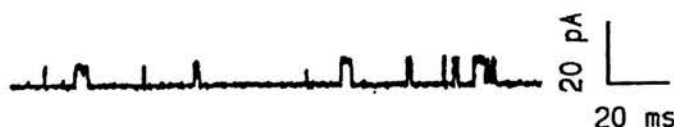


FIGURE 13. Typical trace recorded in the cell-attached configuration at pipette potential $V_p = -60$ mV. The activity reflects openings of large-conductance potassium channels.

As seen in Fig. 13, channels clearly show well defined conformational states (closed and open). Moreover, the time duration of single channel openings shows clear variability indicating the stochastic nature of single channel activity. To describe the single channel openings in terms of stochastic processes, the histograms of dwell time distributions are constructed (Fig. 14). These distributions can be well fitted with probability density functions described by a sum of exponentials indicating Markovian processes.

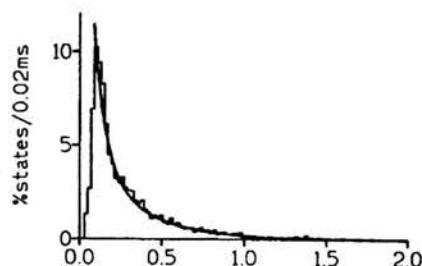


FIGURE 14. Open time distribution for single channel activity presented in Fig. 13. The probability density function fitted to the distribution is a sum of two exponentials.

In the patch-clamp technique, the pipette potential is controlled by the experimenter. Thus this technique offers an advantage to record the I-V characteristics for the single channel currents. Example of such recordings is presented in Fig. 15.

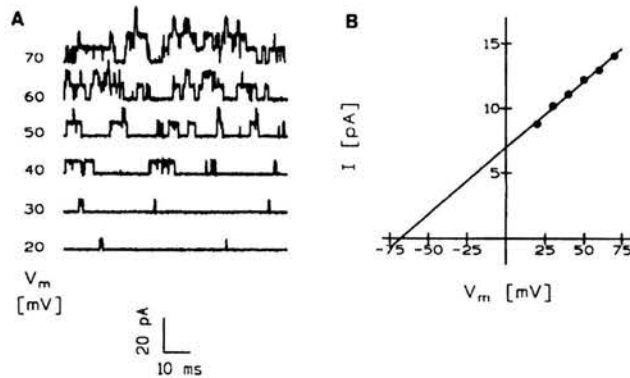


FIGURE 15. Single channel currents recorded at different voltages (panel A). Panel B: I – V relationship for currents presented in the panel A. The relationship is fitted with a straight line the slope of which indicates the single channel conductance [16].

The slope of the I – V relationship indicates the single channel conductance. The conductance of a single channel depends on the channel type but typically is in the range of a few tens of picosimens. The largest channels reach the conductance of 200 pS and the smallest have conductance of a few pS. The extrapolation of the linear fit to the I – characteristics indicates the reversal potential for currents. The comparison of such potential with a predicted value of the Nernst equilibrium potential for considered ions is a most straightforward tool to check the channel selectivity. In the case presented in Fig. 15 reversal potential was close to the equilibrium potential for potassium providing strong evidence that the recorded currents were due to activity of potassium channels.

The single channel recordings clearly demonstrate that functioning of channels relies on stochastic fluctuations between well defined conformational states.

It is interesting to compare the macroscopic currents recorded using the classical voltage-clamp technique (Fig. 7) to the single channel recordings recorded using the patch-clamp technique. The stochastic nature of channel activity is not manifested in macroscopic currents (voltage-clamp experi-

ments, Fig. 7) as current flows through a very large number of channels and therefore the experimenter observes an averaged channel behavior. On the contrary, using the patch-clamp technique, one observes the single channel fluctuations that are quite different from currents observed in the voltage-clamp recordings. However, in order to deduce an average behavior, several single channel recordings can be performed and the recorded currents averaged yielding so-called ensemble averaged current. The result of such a procedure is presented in Fig. 16. The depolarizing pulses applied in the cell-attached configuration evoke the single channel activity of sodium channels. One single channel trace is very different from the other due to stochastic nature of the single channel activity. However, after having performed the ensemble averaging of these currents (bottom trace in Fig. 16) a similar sodium current is observed as in the voltage-clamp experiments. Thus there is a consistent agreement between averaged behavior of single channels and macroscopic current. Thus patch clamp allows us to get an insight into both micro and macroscopic properties of membrane conductance.

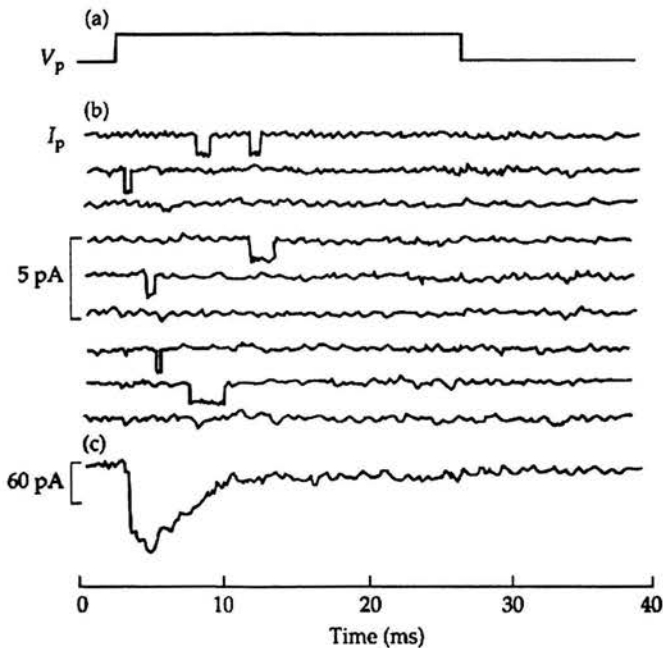


FIGURE 16. Single channel sodium currents evoked by depolarizing stimuli (inset above the single current traces). Averaging of the single channel traces yields the "macroscopic" current similar to those measured in the voltage-clamp experiments (Fig. 7); adopted from [15].

Similar procedure of ensemble averaging can be performed for any other type of channels. For instance, Fig. 17 shows it for large-conductance inactivating potassium channels in chondrocyte. It is worth noting that in the example presented in Fig. 17, channels show considerable inactivation in contrast to delayed rectifier potassium channels in the squid giant axon (Fig. 7). This difference reflects the fact that the voltage-gated potassium channel family is mostly diversified among voltage-dependent ionic channels. In an extreme case, the so-called A type potassium channels show inactivation as fast as in the case of sodium channels. Moreover, in the case of A type potassium channels, their steady-state inactivation at the resting membrane potential is as high as approximately 0.5, meaning that at the resting state about one half of channels are inactivated.

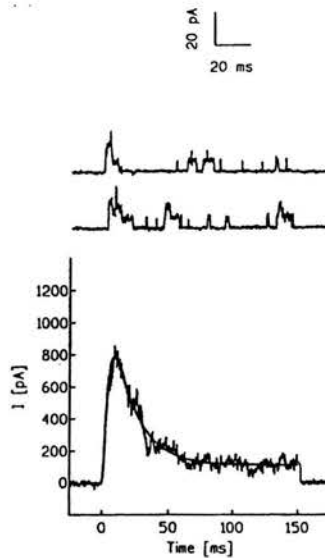


FIGURE 17. Ensemble averaging of single channel traces evoked by square-like depolarizations (similarly to Fig. 17) for single-channel large conductance potassium currents [17].

Configurations of the patch-clamp technique

Besides the cell-attached configuration, the patch-clamp technique can be applied also to several other modes. As shown in Fig. 18, the whole-cell configuration can be obtained after the patch-of the membrane underlying the pipette tip is disrupted. Practically this is achieved by applying a slight suction (a pulse of “negative” pressure) to the pipette. When the membrane

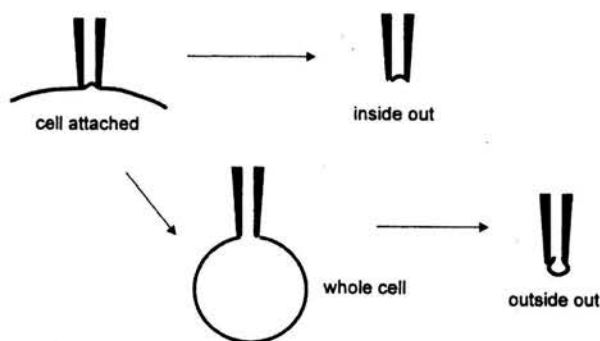


FIGURE 18. Configurations of the patch-clamp technique; adapted from [5].

patch is broken, the electrode has an electrical contact with the interior of the cell and therefore in this configuration it is possible to measure the current flowing through the entire cell membrane while controlling the potential of the whole cell. The whole-cell configuration is practically equivalent to the classical voltage-clamp technique (for this reason it is called sometimes a “single electrode voltage-clamp”). After having established the whole-cell configuration, it is possible to reach an excised outside-out patch configuration. Technically, this configuration is obtained by lifting the pipette upwards and the excised patch is physically detached from the cell in such a way that the external side of the membrane is still in contact with the external solution. The outside-out excised patch configuration is extremely useful in pharmacological studies as it is much easier to exchange the solutions around a small patch than around a whole-cell. When detaching the pipette from the cell in the cell-attached mode, an inside-out excised patch can be obtained. Sometimes when detaching the pipette starting from the cell-attached configuration, a tiny vesicle is formed but a brief air exposure causes a rupture of the external part of the vesicle and the inside out excised patch configuration is obtained.

4. Synaptic transmission

The phenomena described so far concern the properties of a single neuron. Even when the action potential is propagated along a 1 m long axon we need to bear in mind that it is initiated and terminated within the same neuron. The transfer of signal to a different cell (another neuron or muscle fibre) occurs in the synapses. Two types of synapses are distinguished: electrical and chemical. Since in the mature central nervous system, most of fast signaling

occurs via chemical synapses, in the present work I will concentrate our attention on the properties of this type of synapses.

Synaptic transmission (Fig. 19) consists of a sequence of events:

- (i) action potential travels along the axon and "invades" the nerve terminal,
- (ii) depolarization of the presynaptic membrane activates the calcium channels leading to an increase in the intracellular calcium concentration,
- (iii) increased intracellular calcium concentration triggers exocytosis of the synaptic vesicles and release of neurotransmitter into the synaptic cleft,
- (iv) neurotransmitter diffuses across the cleft and get bound to the postsynaptic receptor-channel complex inducing their opening,
- (v) current flow through the postsynaptic ligand-gated channels induces the potential change on the postsynaptic cell membrane.

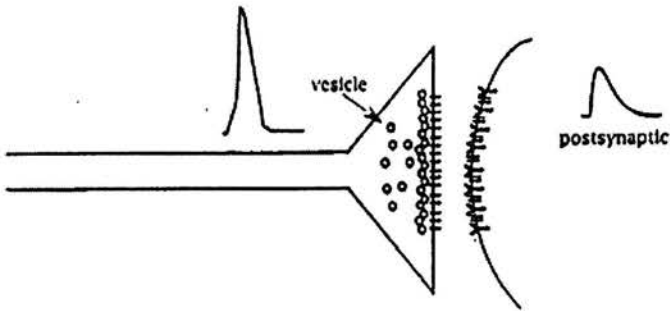


FIGURE 19. Schematic view of a synapse.

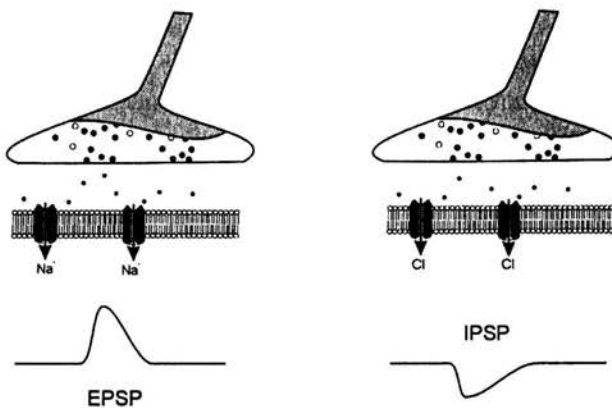


FIGURE 20. Most generally chemical synapses are divided into excitatory and inhibitory.

Most generally, synapses are classified as excitatory and inhibitory (Fig. 20). In the mature central nervous system excitatory synaptic transmission is mediated by glutamic acid while inhibitory synaptic transmission by GABA (brain) and glycine (spinal cord). The type of synapse (inhibitory or excitatory) depends on the type of postsynaptic receptors and on the electrochemical gradient of permeant ions. In brain, the inhibitory transmission is mediated by GABAA receptors while in the spinal cord by glycine receptors and both these receptors are permeant to anions. During early development, the intracellular chloride concentration is much higher than in the adulthood. A consequence of this difference is that in young individuals, the equilibrium potential for chloride is higher than the resting potential while in adults the opposite is present. This implies that the activation of the chloride conductance in developing individuals will result in the membrane depolarization implying that in the early stage of development, somehow paradoxically, GABA and glycine are excitatory neurotransmitters. During the development, the equilibrium potential progressively shifts towards more negative values eventually becoming negative with respect to the resting potential.

The excitatory transmission is mediated by a family of glutamate receptors that will not be described in the present paper as I will focus on inhibitory synaptic transmission.

Conditions of synaptic receptor activation

As mentioned above, during synaptic transmission the neurotransmitter is released into the synaptic cleft and after having reached the postsynaptic membrane activates the ligand gated channels. Obviously, the extent of receptor activation of these receptors depends on time course of synaptic agonist concentration. What is the peak concentration of the agonist in the synapse and for how long the agonist is present in the synaptic cleft? The width of synaptic cleft is very small (approximately 50 nm) and for this reason direct measurement of the agonist concentration time course within the synapse is not possible. Assuming that the neurotransmitter is released very quickly (instantaneous dumping model of release), the time course of concentration profile can be estimated by solving the diffusion equation for the boundary conditions reflecting the geometry of synaptic cleft and for the initial condition consistent with the assumption of immediate dumping model:

$$\frac{\partial c(x, t)}{\partial t} = D \frac{\partial^2 c(x, t)}{\partial x^2}. \quad (4.1)$$

Numerical solutions of such boundary problem indicate that at distances corresponding to the width of the synaptic cleft the time needed for the ag-

onist to reach the postsynaptic membrane is approximately a few microseconds. The clearance of the neurotransmitter is predicted to be a biphasic process characterized by a predominant time constant of a few hundreds of microseconds (Fig. 21). This implies that the synaptic receptors 'see' the neurotransmitter for at most a few hundreds of microseconds. Thus these receptors are activated in conditions of extreme non-equilibrium [18-21]. This information regarding the pattern of receptor activation is of fundamental importance. If we wish to properly describe the mechanisms underlying the time course and pharmacological modulation of the synaptic transmission, the knowledge how the activation of these receptors occur is crucial. Simply, as in the case of any chemical reaction, its kinetics depends on the time course of the substrate concentrations, the synaptic transmission (or its modulation) must depend on the time course of its crucial substrate – neurotransmitter. In addition, this aspect seems particularly important since the major form of activity of the ligand-gated channels is to mediate the synaptic transmission. Thus, although it is much easier to study the properties of these receptor in equilibrium or in a steady-state conditions but referring such results to the synaptic conditions could be problematic.

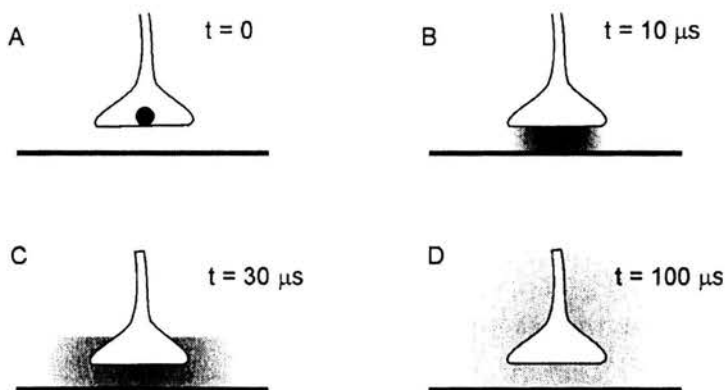


FIGURE 21. Graphical illustration of the neurotransmitter diffusion.

The kinetics of postsynaptic receptors is quite complex

The response of the postsynaptic receptors to the neurotransmitter released from the nerve terminal depends on the receptor kinetics (so-called microscopic gating, Fig. 22).

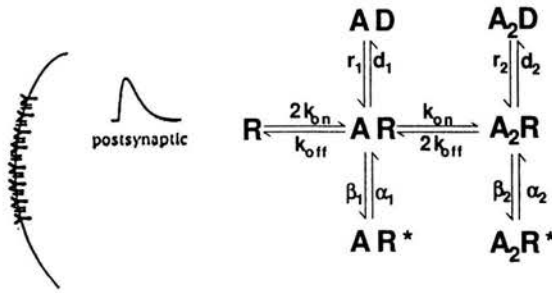


FIGURE 22. Schematic view of the postsynaptic membrane left panel and the scheme describing the receptor kinetics. A – the particles of agonist. R – receptor in the closed state, D – desensitized conformation, R* – receptor in the open conformation.

The considerations presented here will concern from now on, only GABAergic synaptic transmission that is mediated by GABAA receptors and the model presented in Fig. 22, refers to this receptor type [22-23]. It is postulated that receptor may enter one of three conformations: R – closed, R* – open and D – desensitized. In the case of the closed state receptor may be either unliganded or bind one or two agonist molecules. Open state R* may be either singly (AR* or A₂R*) or biliganded. Desensitized state is referred to the receptor conformation in which the channel macromolecule is bound and inactive (does not permeate current) and cannot be activated by ligand application. For most of the ligand-gated channels there is a tendency for the channels to accumulate in the desensitized state during a prolonged exposure to the agonist. However, as we will see later, in the case of GABAA receptors, the desensitized state strongly participates in shaping the synaptic currents. The respective rate constants describe kinetics of transitions between the receptor conformations. It is widely recognized that the entrances into singly bound states (AD and AR*) are very slow and therefore, after agonist application, fully bound states predominate.

Synaptic currents can be routinely recorded using the patch-clamp technique

The synaptic currents are measured in the whole-cell configuration (Fig. 23) of the patch-clamp technique. As described above, in this configuration, the membrane potential is clamped and the current flowing through entire membrane is measured. Thus, if at any of the synapse on the neuron from which the recordings are made, the synaptic transmission occurs, the postsynaptic currents is detected by the recording electrode.

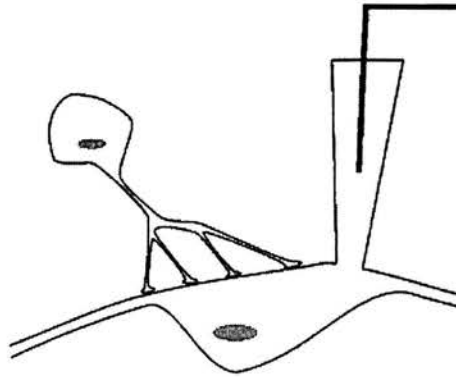


FIGURE 23. Recordings of the postsynaptic currents is performed in the whole-cell configuration of the patch-clamp technique.



FIGURE 24. Typical traces of spontaneous GABAergic synaptic currents recorded at holding potential of -70 mV.

In general, any neuron may receive signals from hundreds of other neurons through thousands of synapses. This illustrates how complex is the process of signal integration on a single neuron. In Fig. 24, typical traces of GABAergic synaptic currents are shown.

It is apparent that the synaptic currents (Fig. 24) are characterized by a large amplitude variability. These differences may result from the fact that various synapses are characterized by different number of the postsynaptic receptors. To some extent this variability could be caused also by different amount of neurotransmitter in synaptic vesicles.

How to determine the kinetics of the postsynaptic GABAA receptors?

Although the synaptic current recordings can be routinely performed in the whole-cell configuration of the patch-clamp technique, such recordings are usually insufficient to describe either the kinetics or the pharmacological modulation of the postsynaptic receptors. The standard approach to address such problems would be to construct the dose-response relationships that may provide the information needed to assess the rate constants in the considered kinetic scheme (Fig. 25). Dose-response relationship, in the case of the activity of ligand gated channels, does not necessarily mean only the concentration-dependence of current amplitudes but usually it is referred also to the kinetic features of currents (for instance activation time, deactivation kinetics, desensitization kinetics, frequency of channel openings, etc., see below) In the case of kinetics of the chemical reactions, the velocity of the

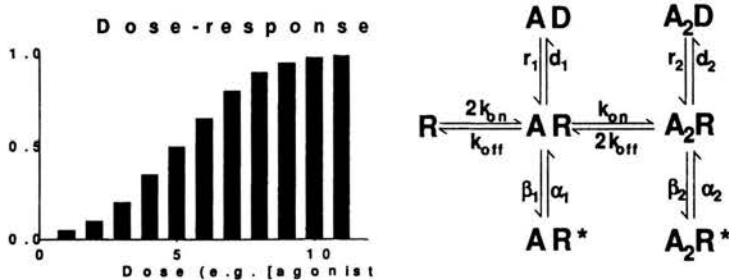


FIGURE 25. Exemplary dose-response relationship and the considered kinetic model.

product reaction is monitored while a substrate concentration is varied and in this way the information on the reaction kinetics is obtained. It seems thus logical to implement a similar approach to study the kinetics of the postsynaptic receptors. However, the synaptic currents represent current responses to basically unknown agonist concentration. Moreover, it is impossible to effectively manipulate over a wide range the concentration of neurotransmitter released in synapse. This implies that that in the case of synaptic current recordings, the standard approach based on the analysis of the dose-response relationships cannot be used and this is the main reason for which synaptic currents provide too little information to describe the pharmacokinetics of the postsynaptic receptors.

Current responses to exogenous GABA applications reveal the kinetics of GABAA receptors

A possibility to bypass the difficulties encountered when analyzing the synaptic currents would be to record the current responses to exogenous GABA applications. By collecting such responses to different GABA concentrations, the dose-response relationships can be constructed. However, in order to make such investigations relevant to synaptic transmission, the agonist need to be applied sufficiently fast to mimic the conditions of synaptic receptor activation. In practical terms this means that the agonist should appear in the closest vicinity of the studied membrane within at most hundreds of microseconds. From the technical point of view this means that the application system must be able to physically exchange the solution around the membrane within much less than 1 ms. This prerequisite set considerable limits for the pharmacokinetic studies of ligand-gated channels for long decades. In the early nineties first Joseph Dudel and then Peter Jonas have designed the ultrafast perfusion system able to exchange the solution around the cell membrane within less than 100 microseconds [24, 25].

Ultrafast perfusion system allows to apply agonist with similar velocity as in synapse

The main device in the ultrafast perfusion system is the piezoelectric driven theta-glass pipette. The so-called theta-glass (Fig. 26) is a cylindrical capillary divided symmetrically by a septum. Thus the theta-glass may eject two different solutions that outside the theta tube form a laminar flow (Fig. 27).

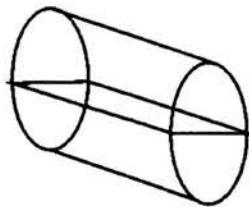


FIGURE 26. 'Theta-glass' capillary.

The theta-glass is mounted on a piezoelectric translator that can very quickly move down or upward. As shown in Fig. 27, the pipette with an excised patch can be washed either with a normal saline or with solution with a selected concentration of agonist. The time of agonist exchange using this

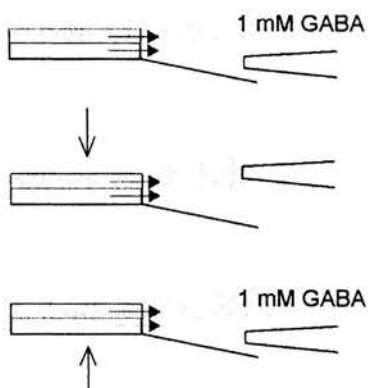


FIGURE 27. Downward and upward translation of theta glass moves the laminar fluxes of solutions. In this way the excised patch on the patch pipette can be washed by normal saline (upper figure), then suddenly, following the downward translation of theta-glass, the excised patch is exposed to the chosen agonist concentration (middle figure). The movement of the theta-glass upward restores the washing solution around the patch.

system can be as short as approximately 50 microseconds implying that this technique enables us to mimic the speed of agonist application in the synapse. To see whether the use of ultrafast perfusion system allows to mimic the synaptic conditions, one can compare a current response to short application of agonist and synaptic current. Such comparison is shown in Fig. 28.

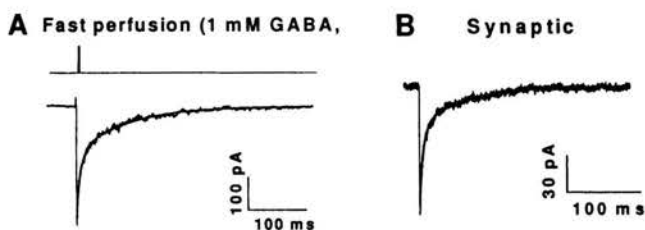


FIGURE 28. Comparison of current response to a brief (1 ms), ultrarapid GABA application to a synaptic current. Inset above the current trace in (A) represent the time of agonist application. Both currents are recorded at -70 mV.

As shown in Fig. 28 the current responses to ultrafast GABA application closely resembles the synaptic current (Fig. 28B). Both are characterized by

a rapid onset and a slower decay (these are inward, i.e. negative currents and onset and decay mean here activation phase and return to baseline, respectively). This simple comparison provides the first and very important evidence that synaptic currents result from a very rapid and brief application of agonist.

5. Tracing the gating of ligand gated ion channels

As discussed above, the ultrafast perfusion system provides the means to study the kinetics of ligand-gated channels in the time scale adequate to synaptic transmission. Besides the fact that it enables us to mimic the synaptic currents (Fig. 28), it offers a crucial advantage that an experimenter can construct the dose-response relationships for current responses evoked by GABA applications sufficiently fast to reasonably restore the synaptic conditions. Below I present exemplary investigations aiming at resolving the kinetics of GABAA receptors. For this purpose, the frame of Jones and Westbrook's kinetic scheme was used, cf. (Fig. 22).

Since the seventies it has been recognized that the activation of ligand-gated channels consists of two main steps: binding of neurotransmitter to the binding sites on channel macromolecule and the conformational transition from the bound closed (A_2R) to bound open state (A_2R^*), cf. [26]. There is a general agreement that there are two binding sites on GABAA receptor. The only ligand-dependent step (i.e. dependent on agonist concentration) is binding and the speed of conformational transitions between the bound states do not depend on agonist concentration. Assuming the first order reaction for binding, the effective rate of binding is proportional to GABA concentration:

$$\text{effective binding rate} = k_{\text{on}} \cdot [\text{GABA}], \quad (5.1)$$

where k_{on} denotes the binding rate and $[\text{GABA}]$ is the concentration of GABA.

If agonist concentration is low, then binding is slow and rate limiting. On the contrary, at high $[\text{GABA}]$ at which binding is faster than conformational transition, the rate limiting factor in the activation process is the transition from closed (A_2R) to open (A_2R^*) state. It is thus expected that at sufficiently low $[\text{GABA}]$, the activation kinetics represented by the onset of current response, will be strongly dependent on agonist concentration. Figure 29 shows the dependence of current onset on the concentration of applied GABA. It needs to be stressed that although the onset of responses is fast, the exchange time of ultrarapid perfusion system used here is much faster (approximately 50 microseconds) meaning that the observed differences in the rise times do represent the differences in the channel kinetics.

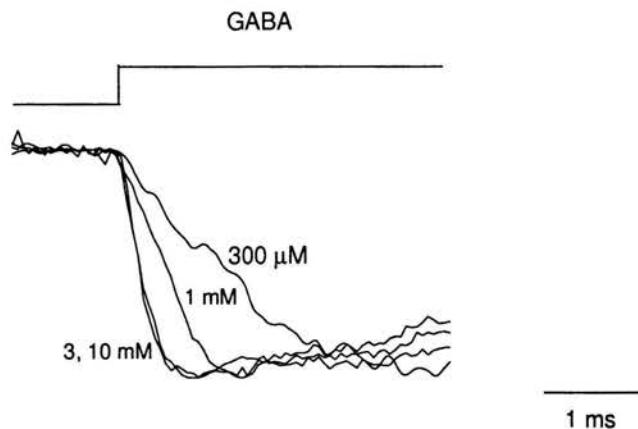


FIGURE 29. Dependence of current rising phase on applied GABA concentration.

When increasing $[GABA]$ from $300\ \mu\text{M}$ up to $3\ \text{mM}$, the current onset accelerate that is consistent with the increase in binding rate (Eq. (5.1)). However, above $3\ \text{mM}$ GABA, the current rise time does not accelerate any more. This reflects the fact that binding becomes much faster than closed to open transition and this conformational change (that is ligand-independent) becomes rate limiting. Thus above $3\ \text{mM}$, the receptor activation reaches saturation and therefore doses of GABA above $3\ \text{mM}$ are often defined as saturating. We observe that such dose-response relationship (i.e. dependence of rising phase on $[GABA]$) provides important information on the binding rate of GABA (k_{on}). The rise time of current response to saturating $[GABA]$ is very fast (approximately $0.25\ \text{ms}$). This implies that as soon as the receptor binds the agonist its "time of reaction" is very short. Taking additionally into account that, as discussed above, the diffusion of neurotransmitter is very rapid, the entire process of signal transduction in the GABAergic synapse is very fast.

In the scheme, also singly liganded open (AR^*) and desensitized (AD) states are included but the rate of entrance into these states (β_1 and d_1) are very small and relatively important contribution of these states to the overall receptor activity may occur only at low $[GABA]$.

Decay of synaptic current represents the deactivation process

The recordings of current response presented in Fig. 28 show that after withdrawal of agonist the current does not fall immediately to zero but shows a relaxation. Such current time course after removal of the agonist is defined as deactivation. Since the agonist is present in the synaptic cleft for a very

short time, the decay of synaptic current may be regarded as the deactivation process. Thus deactivation plays a crucial role in setting the time duration of the synaptic currents and it is important to understand the mechanisms determining the time course of this process. It needs to be emphasized that in the case of GABAergic synaptic currents, the deactivation process is as slow as hundreds of milliseconds that is nearly one order of magnitude longer than the single channel opening. Jones and Westbrook (1995) in their thorough study on this subject have provided a convincing explanation why the deactivation of the GABA-elicited currents shows so slow kinetics. According to the Jones and Westbrook's model (Fig. 22), after a brief (e.g. 1 ms) application of saturating concentration of GABA, the binding process proceeds very quickly and within at most a few hundreds of milliseconds, most of receptors reach the fully bound state and then open or "fall" into the desensitized state. After a period of time spent in the open or desensitized state receptor returns to the closed bound state (A_2R). If the unbinding rate k_{off} is slow, then before the receptor dissociate the agonist the channel may re-enter the open or desensitized state. Thus a slow unbinding may favor multiple entrances into open and desensitized conformation giving rise to prolongation of the deactivation process. Thus, somehow paradoxically, desensitization state strongly participates in shaping the synaptic currents. This observation is supported by the single channel recordings (Fig. 30).

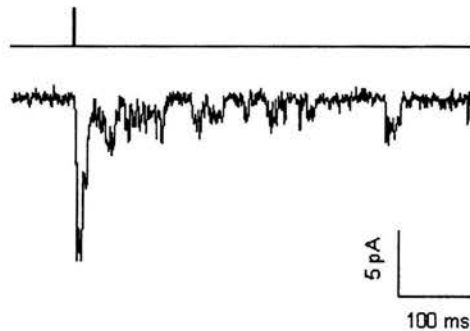


FIGURE 30. Current response elicited by brief (2 ms) application of 10 mM GABA. Agonist induces activation of channels (peak) but after its removal single channel openings separated by silent periods are observed.

We observe that after agonist removal (Fig. 30), channel openings are observed indicating that a proportion of channels remained in bound conforma-

tion. Moreover, the silent periods that separate the single channel openings indicate "visits" in the desensitized state.

Such functional link between desensitization opening and unbinding have been consistently confirmed by additional experiments. If the above explanation is correct in an analogous experiment performed using low affinity agonist (i.e. with faster k_{off}), the deactivation process is expected to be much faster than in the case of GABA. Indeed, as shown in Fig. 31, when applying a short pulse of 100 mM of β -alanine, the deactivation process markedly accelerates. This difference does not result from a shortening of the single channel opening (that are similar for both agonists) but from the inability of multiple entrances into the open and desensitized states in the case of β -alanine.

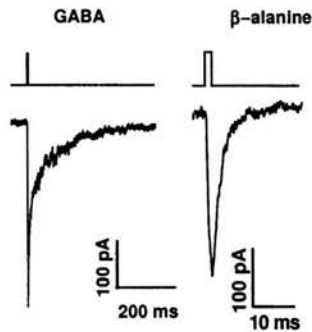


FIGURE 31. Comparison of the deactivation kinetics of current responses to GABA and β -alanine.

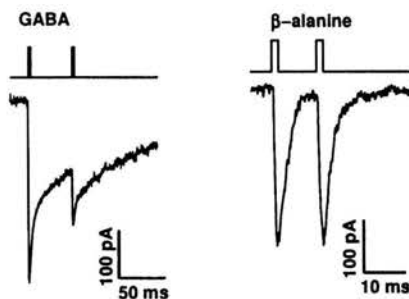


FIGURE 32. Current responses to pairs of brief pulses of saturating GABA and β -alanine. Note that in the case of GABA, the current elicited by the second pulse is smaller than the first one indicating that during the interpulse interval an accumulation in the desensitized conformation occurred.

Another evidence of functional coupling between desensitization, opening and unbinding came from so-called double-pulse experiments (Fig. 32).

Suppression of the second peak in the double pulse experiment using GABA can be consistently explained as a consequence of slow unbinding. Thus, after application of the first pulse due to slow k_{off} , the receptors remain for a period of time in the bound conformations oscillating between open, closed and desensitized state. Since the exit from desensitization (τ_2) is much slower than the entrance d_2 , a progressive accumulation in the desensitized state occur and the response to the second GABA application is smaller (a part of receptors is "trapped" in the desensitized conformation). However, in the case of low affinity agonist (β -alanine), the unbinding rate is sufficiently fast to preclude multiple entrances and accumulation in the desensitized state. Simply, the receptor that closes (enters the A_2R state) after a stay in the open state (A_2R^* state) quickly dissociates the agonist molecule due to very fast unbinding rate precluding the entrance into the A_2D state. This is why in the case of β -alanine, there is no paired pulse inhibition.

Current responses to long pulses of GABA reveal the kinetics of desensitization onset

Long applications of high agonist concentrations are known to favor accumulation of receptors in the desensitized state (Fig. 33, accumulation in the desensitized state is visualized by the decay following the peak).

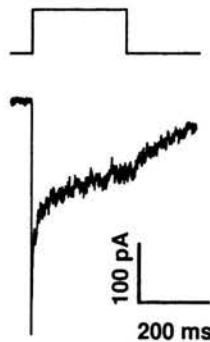


FIGURE 33. Long applications of saturating GABA concentration induces the accumulation in the desensitized conformation.

The “route” of this process can be followed using the Jones and Westbrook’s model (Fig. 22). Thus, after application of high concentration of agonist the receptors bind the neurotransmitter, a part of receptors open (A_2R^*) and a part enter directly into the desensitized state (A_2D). Thus, the peak of measured current represent the proportion of receptors that entered into the open state without visiting the desensitized state before. After the period of time equivalent to the mean open duration, the channel returns to the closed conformation (A_2R). However, due to persistent presence of high concentration of the agonist, the receptor remain in the bound state that increases the probability of being absorbed by the desensitized state. The desensitization onset can be well described by a sum of two exponentials with time constants (τ_{fast} of ca. 2 – 3 ms and τ_{slow} ca. 100 ms) indicating the presence of two desensitized states with different kinetics. However, the slow component is unlikely to significantly shape the synaptic currents and for this reason, in the Jones and Westbrook’s model, only one (fast) fully bound state is considered.

Model simulations allow to quantify and interpret experimental findings

The description of the receptor gating requires determination of the rate constants in the considered model (in the present case the scheme in Fig. 22). The optimization procedures are performed until the set of the rate constants allows to best reproduce the kinetic behavior observed in all the protocols employed. The current observed in the experiments described above, in model simulations (Figs. 34 and 36) are represented by a total occupancy of the open states (except for the case of very low [GABA], the occupancy of the fully bound state A_2R^* is predominant).

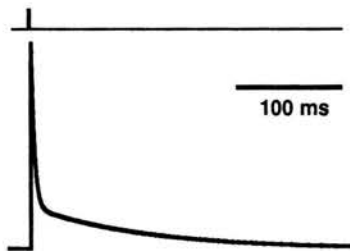


FIGURE 34. Simulation of current response to a brief pulse (1ms) of saturating GABA (10 mM).

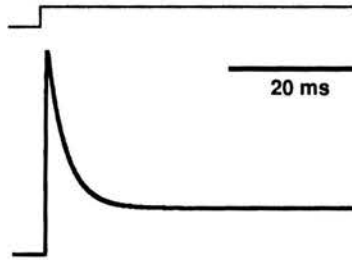


FIGURE 35. Simulation of current response to long application of saturating GABA.

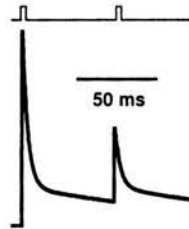
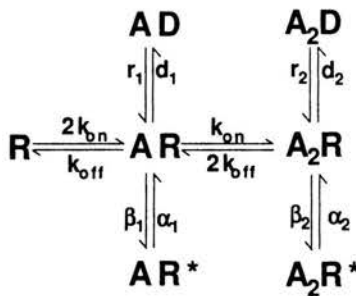


FIGURE 36. Simulations of current responses to rapid application of GABA in double pulse experiment (short pulses). Note paired pulse inhibition. The simulations are performed for the parameters presented in Table 5.9.



Param.	value
k_{on} [$\text{ms}^{-1}\text{mM}^{-1}$]	6.0
k_{off} [ms^{-1}]	1.0
β_1 [ms^{-1}]	0.15
α_1 [ms^{-1}]	1.5
d_1 [ms^{-1}]	0.045
r_1 [ms^{-1}]	0.014
β_2 [ms^{-1}]	3.0
α_2 [ms^{-1}]	0.4
d_2 [ms^{-1}]	12.0
r_2 [ms^{-1}]	0.07

FIGURE 37. Values of the rate constants used in model simulations (Figs. 34 and 36). This set of parameters allowed to optimally reproduce the experimental data showed above.

6. Concluding remarks

The above presented examples of electrophysiological investigations were chosen to demonstrate how powerful can be a combination of a sophisticated experimental approach associated with a thorough quantitative investigations. In biological sciences there are few examples in which such combination gave such important contribution to understanding basic physiological phenomena. As already mentioned, the Hodgkin and Huxley equations first shed light on the mechanisms underlying the excitability and at the same time became an everyday tool in electrophysiological investigations. The investigation by Hodgkin and Huxley provide a paramount example that even the most clever experimental approach is not sufficient to explore the nature of studied process – good techniques allow to collect high quality data but their elaboration based on quantitative models allows to understand them.

The rapid development of various forms of the patch-clamp technique together with the application techniques enabled the electrophysiologists to greatly improve the resolution of neuronal signaling. Again, successful recordings of currents at resolution adequate to synaptic transmission prompted the model simulation to explore the mechanisms underlying the kinetics and pharmacological modulation of this phenomenon. The presented experimental and analytical approach became a standard for a wide spectrum of problems related to the synaptic transmission. The next step will be to implement a similar strategy in an attempt to understand the channel functioning at the molecular level.

Acknowledgements

This work was supported by the State Committee for Scientific Research (KBN, Poland) through the grant No 6 P04A 001 19. The author wishes to thank Dr. Andrzej Hendrich for his help in preparing many of the figures presented in this work.

References

1. E.R. KANDEL, J.H.SCHWARTZ, T.M.JESSEL (Eds.), *Principles of Neural Sciences*, Elsevier, New York, 1991.
2. B. HILLE, *Ionic Channels of Excitable Membranes*, Sinauer Associates INC, 1992.
3. H.C. TUCKWELL, *Introduction to theoretical neurobiology*, Cambridge University Press, 1988.
4. K.S. COLE, H.J. CURTIS, Electric impedance of squid giant axon during activity. *Journal of General Physiology*, Vol.22, pp.649-670, 1939.

5. S. MIĘKISZ, A. HENDRICH, *Wybrane zagadnienia z biofizyki*, Volumes, Wrocław, 1998.
6. A.L. HODGKIN, A.F. HUXLEY, Resting and action potentials in single nerve fibres, *Journal of Physiology*, Vol.104, pp.176-195, 1945.
7. A.L. HODGKIN, A.F. HUXLEY, Currents carried by sodium and potassium ions through the membrane of the giant axon of Loligo, *Journal of Physiology*, Vol.116, pp.449-472, 1952.
8. A.L. HODGKIN, A.F. HUXLEY, The components of membrane conductance in the giant axon of Loligo, *Journal of Physiology*, Vol.116, pp.473-496, 1952.
9. A.L. HODGKIN, A.F. HUXLEY, The dual effect of the membrane potential on sodium conductance in giant axon of Loligo, *Journal of Physiology*, Vol.116, pp.497-506, 1952.
10. A.L. HODGKIN, A.F. HUXLEY, A quantitative description of membrane current and its application to conduction and excitation in nerve, *Journal of Physiology*, Vol.117, pp.500-544, 1952.
11. B. KATZ, R. MILEDI, Membrane noise produced by acetylcholine, *Nature*, Vol.226, pp.962-963, 1970.
12. B. KATZ, R. MILEDI, Further observations on acetylcholine noise, *Nature*, Vol.232, pp.124-126, 1971.
13. C.R. ANDERSON, C.F. STEVENS, Voltage-clamp analysis of acetylcholine produced endplate current fluctuation at frog neuromuscular junction, *Journal of Physiology*, Vol.235, pp.655-691, 1973.
14. E. NEHER, B. SAKMANN, Single channel currents recorded from the membrane of denervated frog muscle fibres, *Nature*, Vol.260, pp.260:779-802, 1976.
15. J.G. NICHOLLS, A.R. MARTIN, B.G. WALLACE, P.A. FUCHS, *From Neuron to Brain*, Sinauer Associates, 2001.
16. J.W. MOZRZYMAS, M. VISINTIN, F. VITTUR, F. RUZZIER, Potassium channels of pig articular chondrocytes are blocked by propofol, *Biochemical and Biophysical Research Communications*, Vol.202, pp.31-37, 1994.
17. J.W. MOZRZYMAS, M. MARTINA, F. RUZZIER, A large conductance voltage-dependent potassium channel in cultured pig articular chondrocytes, *Pflugers Archiv - European Journal of Physiology*, Vol.433, pp.413-427, 1997.
18. J.D. CLEMENTS, Transmitter time course in the synaptic cleft: its role in central synaptic function, *Trends in Neuroscience*, Vol.19, pp.163-170, 1996.
19. J.W. MOZRZYMAS, A. BARBERIS, K. MICHALAK, E. CHERUBINI, Chlorpromazine inhibits Miniature GABAergic currents by Reducing the Binding and by Increasing the Unbinding Rate of GABA_A Receptors, *Journal of Neuroscience*, Vol.19, pp.2474-2488, 1999.
20. A. BARBERIS, E. CHERUBINI, J.W. MOZRZYMAS, Zinc inhibits miniature GABAergic currents by allosteric modulation of GABA_A receptor gating, *Journal of Neuroscience*, Vol.20, pp.8618-8627, 2000.
21. J.W. MOZRZYMAS, A. BARBERIS, K. MERCIK AND E.D. ZARNOwsKA, Binding sites cooperativity, singly bound states and conformation coupling shape GABA-evoked currents, *Journal of Neurophysiology*, Vol.89, pp.871-883, 2003.

22. M.V. JONES, G.L. WESTBROOK, Desensitized states prolong GABA_A channel responses to brief agonist pulses, *Neuron*, Vol.15, pp.181-191, 1995.
23. M.V. JONES, G.L. WESTBROOK, Shaping of IPSCs by endogenous calcineurin activity, *Journal of Neuroscience*, Vol.17, pp.7626-7633, 1997.
24. P. JONAS, Application of agonists to isolated membrane patches, in: B. Sakmann and E. Neher (Eds.), *Single Channel Recordings*, pp.231-242, Plenum Press: New York and London, 1995.
25. C. FRANKE, J. DUDEL, Liquid filament switch for ultra-fast exchanges of solutions at excised patches at synaptic membranes of crayfish muscle, *Neuroscience Letters*, Vol.77, pp.199-204, 1987.
26. K.L. MAGLEBY, C.F. STEVENS, A quantitative description of end-plate currents, *Journal of Physiology*, Vol.223, pp.173-197, 1972.

